Stable Sustainment of Plasmas with Electron Internal Transport Barrier by ECH in the LHD

Y. Yoshimura[1], H. Kasahara[1], M. Tokitani[1, 2], R. Sakamoto[1, 2], Y. Ueda[3], N.B. Marushchenko[4], R. Seki[1, 2], S. Kubo[1], T. Shimozuma[1], H. Igami[1], H. Takahashi[1, 2], T.I. Tsujimura[1], R. Makino[1], S. Kobayashi[1], S. Ito[1], Y. Mizuno[1], K. Okada[5], T. Akiyama[1], K. Tanaka[1], T. Tokuzawa[1], I. Yamada[1], H. Yamada[1, 2], T. Mutoh[6], Y. Takeiri[1, 2], and the LHD Experiment Group

[1]National Institute for Fusion Science, National Institutes of Natural Sciences, Toki, Japan

[2]The Graduate University for Advanced Studies SOKENDAI, Department of Fusion Science, Hayama, Japan

[3]Graduate School of Engineering, Osaka University, Osaka, Japan

[4] Max Planck Institute for Plasma Physics, EURATOM Association, Greifswald, Germany

[5]Nagoya University, Nagoya, Japan

[6]Chubu University, Kasugai, Japan

E-mail contact of main author: yoshimura.yasuo@LHD.nifs.ac.jp

Abstract. The long pulse experiments in the LHD has made progress in sustainment of improved confinement states. It was found that steady-state sustainment of the plasmas with improved confinement at the core region, that is, electron internal transport barrier (e-ITB), was achieved with no significant difficulty. Sustainment of a plasma having e-ITB with the line average electron density n_{e_ave} of 1.1×10^{19} m^{-3} and the central electron temperature T_{e0} of ~3.5 keV for longer than 5 min only with 340 kW ECH power was successfully demonstrated.

1. Introduction

The Large Helical Device (LHD) [1−3] in the National Institute for Fusion Science (NIFS) is furnished with superconducting coils and has great advantages in stable and long pulse plasma sustainment. In contrast to tokamaks, the magnetic field configuration for plasma confinement in the LHD is completely generated by superconducting helical and poloidal coils so that excitation of toroidal plasma current is not required. Therefore, the LHD is suitable for performing investigations on issues such as heat removal and plasma-wall interaction, which require stable long pulse discharges without the difficulty of plasma current sustainment. Those investigations are necessary and profitable for future steady state operation (SSO) of up to 1,000 s as planned in the International Thermonuclear Experimental Reactor (ITER) [4].

Long pulse discharges of up to 1 hour have been investigated through intensive studies that use ion cyclotron heating (ICH) with electron cyclotron heating (ECH) in LHD [5−8], setting the first goal as 1 hour sustainment of plasmas with n_{e_ave} at least 1×10^{19} m^{-3}. As the most successful achievement to date, a discharge of 48 minutes with n_{e_ave} of 1.2×10^{19} m^{-3}, and T_{e0} and T_{i0} of 2 keV was performed with 940 kW ICH and 240 kW ECH [3, 8]. As the record for long pulse discharges, the Tore Supra tokamak achieved the highest parameter of n_{e_ave} = 1.8×10^{19} m^{-3}, T_{e0} = 4.8 keV, and T_{i0} = 2.0 keV. However, the pulse duration time T_p was ~6 min [9]. Most recently, the EAST tokamak achieved stable sustainment of a plasma with high confinement state (H-mode with $H_{98(y2)}$ ~ 1.1−1.2) for ~60 s [10, 11]. On the other hand, as a stellarator, the LHD plasma is excellent at T_p of up to 54 min, and the plasma parameter shows significant improvements in recent years. In addition, long pulse discharges

sustained only with the ECH have been investigated in LHD [12−15], because ECH is considered to be unique and the most reliable heating technique for the future fusion reactors. The highest record of the long pulse plasma sustained with ECH in LHD is $n_{e\_ave} = 1.1\times10^{19}$ m^{-3}, T_{e0} ~2.7 keV, and $T_{i0} = 1$ keV for $T_p = 39$ min [15].

Trials of long pulse discharges in the LHD suggest that the major cause of termination of the discharges with the total heating power of up to ~2 MW is influx of carbon released mainly from around divertors made with carbon. The above-mentioned ECH 39 min discharge was also terminated by carbon influx. In the discharges with higher total power, the major causes of termination are gradual and uncontrollable increase of the electron density attributed to outgas from locally heated inner-vessel components, together with the carbon influx. To eliminate the problem of the carbon influx, adopting metal or metal-coated divertors would be required.

Studies on formation of electron internal transport barrier (e-ITB) or core electron-root confinement (CERC) have been conducted in LHD [16, 17]. Precise on-axis ECH power deposition results in the formation of e-ITB, having threshold absorbed power against the electron density. However, these investigations were performed with pulse lengths shorter than 1 s. Possible causes that have long time constants such as current diffusion (> 10 s in LHD) and/or impurity accumulation may degrade the transport barrier. In Ref. 11, the generation of e-ITB by application of on-axis ECH to the ~60 s H-mode discharge in EAST is briefly reported. However, long pulse sustainment of improved confinement state is not an obvious matter. It should be validated experimentally whether the e-ITB state can be sustained stably as plasmas with normal confinement state, at least until the perturbation by the carbon influx occurs. In this paper, research and experimental activities regarding the topic of sustaining long pulse discharges having e-ITB by ECH, under the limitation of available ECH power sources (gyrotrons) and power injection antenna systems in the LHD, are described as follows. Section 2 describes the LHD and experimental apparatuses, and discusses improvements to these devices undertaken in recent years. Achievement of a stable discharge of longer than 5 min having e-ITB that use EC-waves is introduced in Sec. 3. The paper is then summarized in Sec. 4.

2. Experimental setup

2.1. LHD

The LHD is a helical device with toroidal period number $m = 10$ and polarity $l = 2$. The magnetic field structure including rotational transform for plasma confinement is completely generated by external superconducting magnets, such as a pair of helical coils and three pairs of poloidal coils. The magnetic axis position R_{ax} of LHD plasmas can be adjusted in the range from 3.42 to 4.1 m. In the typical case of $R_{ax} = 3.6$ m, the averaged minor radius is 0.58 m, the plasma volume is 30 m^3, and the maximum magnetic field at the magnetic axis averaged in the toroidal direction, B_t, is 2.85 T. The LHD had two vacuum pumping systems in the period when the ECH long pulse discharges described in this paper were performed. Cryosorption pumps and turbo pumps were installed in the vacuum pumping ports. The cryosorption pumps were not operated and only the turbo pumps (two groups with pumping speed of 6 m^3/s and 15 m^3/s for helium) were operated in the discharges. It is known that even with the operating cryosorption pumps, the main pumping mechanism during discharges is wall-pumping not only in the short pulse discharges of a few seconds but also in the long pulse discharges of a few tens of minutes [18].

2.2. ECH system on the LHD

The current ECH system on the LHD has six working gyrotrons. The oscillation frequencies are 77 (three gyrotrons), 154 (two gyrotrons), and 82.7 (one gyrotron) GHz. The gyrotrons are installed in the heating equipment room next to the LHD hall. The gyrotrons and the LHD are connected with evacuated waveguide power transmission lines. The length of each transmission line is ~100 m. The fundamental (2nd harmonic) resonance magnetic field at the frequency of 77 (154) GHz is 2.75 T. The

77 and 154 GHz gyrotrons have been developed by collaboration with the University of Tsukuba and were installed on the LHD ECH system in recent years. Each of the 77 and 154 GHz gyrotrons generates more than 1.0 MW port-through power at pulse operation of up to a few seconds. Though the nominal output power at continuous wave (CW) operation of the gyrotrons is 0.3 MW or 0.5 MW, the port-through powers in long pulse discharges are suppressed to less than 0.2 MW in order to assure stable and safe operation.

The antenna systems in a top port (5.5-U for 77GHz#3 gyrotron) and in an equatorial port (2-O) are used for the 77 and 154 GHz power injections. In the 2-O port, four antenna systems (2-OLR for 77GHz#1 gyrotron, 2-OLL for 154GHz#1 gyrotron, 2-OUR for 77GHz#2 gyrotron, and 2-OUL for 154GHz#2 gyrotron) are installed. A schematic view of the 2-O port and the four antenna systems is seen in Fig. 1. The upper two antennas, 2-OUR and UL, were newly constructed in 2014 corresponding to the increase in the number of gyrotrons, and were added to the previously installed lower two antennas LR and LL. Therefore, gyrotrons and antenna systems available for recent experiments depend upon the gyrotron installation and the antenna construction.

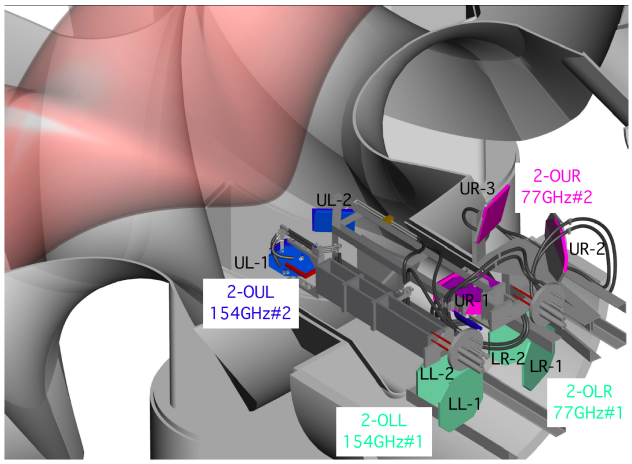

Figure 1. A schematic view of four EC-wave beam injection antenna systems in the LHD 2-O port: 2-OUR (Upper-Right) antenna for 77GHz#2 gyrotron, 2-OUL (Upper-Left) for 154GHz#2 gyrotron, 2-OLR (Lower-Right) for 77GHz#1 gyrotron, and 2-OLL (Lower-Left) for 154GHz#1 gyrotron. The upper two systems were newly installed. Each "-1" mirror is the steerable plane mirror for EC-wave beam direction control. A plasma is drawn in orange color.

The 77 GHz gyrotrons suffer gradual increases of internal pressure during long pulse operation delivering power to LHD. Thus, long pulse operation is limited up to ~ 10 min. For longer pulse experiments, special operation schemes for gyrotrons, such as alternating operations, are required. On the other hand, each of the 154 GHz gyrotrons works well for long pulse operation without noticeable increase of internal pressure due to its short wavelength reducing wave diffraction inside the gyrotron tube and the furnished sub-window to remove stray wave power inside the tube.

3. Stable sustainment of a plasma having electron internal transport barrier by ECH

Plasmas with the improved electron confinement state, e-ITB (or, core electron-root confinement CERC) [16, 17], have been investigated with short pulse discharges (< 1 s) in the LHD. Effective on-axis heating with the increased P_{ECH} at long pulse realized exploration of the possibility of long pulse sustainment of high performance plasmas having e-ITB, without negative effects of impurity accumulation and/or current diffusion. Thus, a long pulse plasma experiment with the condition for precise on-axis ECH was attempted. The working gas was helium supplied with gas puffing systems. The line average electron density is measured with far-infrared interferometer, and the electron temperature and density profiles are measured with Thomson scattering system. In the discharges with pulse length of longer than 10 s, some of the plasma parameters such as plasma stored energy and plasma current are not available due to a drift effect on the integrators in the data processing circuits. The ECH systems of the 77GHz#1 gyrotron (power injection using 2-OLR antenna), 154GHz#1 gyrotron (2-OLL), and 77GHz#3 gyrotron (5.5-U) were available for that experiment. The EC-waves from the 2-O port were injected with toroidally oblique paths, and the EC-wave from the 5.5-U port was injected with a nearly vertical path. Considering the Doppler-shifted on-axis resonance condition for the toroidally oblique injections from 2-O port using TRAVIS code [19], a magnetic field configuration of R_{ax} = 3.65 m with B_t = 2.712 T was set. The beam paths from 2-O port in the

configuration, projected on plasma poloidal cross sections, are calculated and plotted in Fig. 2. Though the cold fundamental and second harmonic resonance layers of 2.75 T (purple lines) are off-axis at $\rho \sim 0.1$, the positions of power deposition (red areas) shift toward low field side and are expected to be nearly on-axis, due to the Doppler effect. The TRAVIS code is useful for pre-experiment investigations and for investigations of long pulse discharges because the code does not inevitably require experimentally obtained three-dimensional equilibrium mapping files (TSmap in the LHD [20]) which are not available for the long pulse discharges due to a lack of measurements, such as the plasma stored energy and the plasma current.

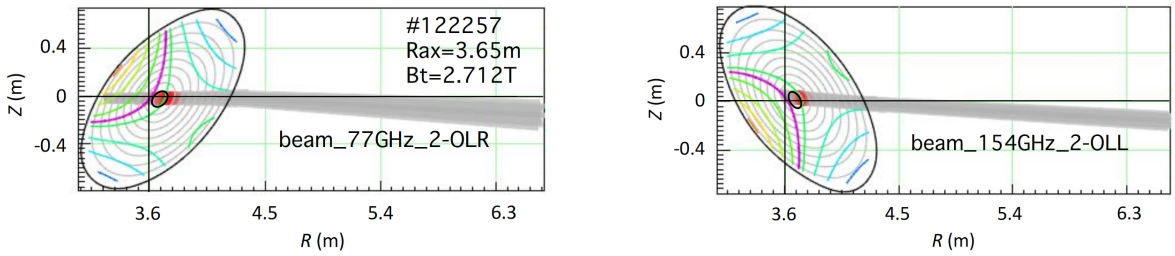

Figure 2. Results of EC-wave ray-tracing calculation by TRAVIS code, for the 77 GHz beam injected from 2-OLR antenna (left) and for the 154 GHz beam from 2-OLL antenna (right) with the configuration of the magnetic field and EC-wave beam directions in #122257. Layers of magnetic field of 2.75 T for fundamental resonance for 77 GHz and second harmonic resonance for 154 GHz are drawn with purple lines. Ellipse-like lines denote the magnetic flux surfaces, and the innermost thick line denotes $\rho = 0.1$. Power deposition regions are colored in red.

Figure 3 shows the waveforms of P_{ECH}, n_{e_ave}, T_{e0}, the electron temperature profile, and the electron density profile of the discharge #122257 in which stable long pulse sustainment of e-ITB longer than 5 min was successfully demonstrated. On the right side of Fig. 3, waveforms of radiation power measured with an absolute extreme ultraviolet diode detector, spectroscopy signals from carbon (CIII) and iron (FeXVI) are also plotted. EC-waves from three gyrotrons, each with continuous ~110kW port through power, were applied for plasma heating. The plasma parameters of $n_{e\_ave} = 1.1\times10^{19}$ m^{-3} and $T_{e0} = \sim3.5$ keV were maintained for 330 s by P_{ECH} of 340 kW. As seen in Fig. 3 (c), the T_e profile has fine ITB structure and the profile is maintained stably throughout the discharge duration.

The radiation power and the impurity signals show no increase or accumulation during the 5 min discharge, except for the sharp increases at the timing of termination, as seen in Fig. 3 (d), (e), and (f). The behaviour of the impurity signals of FeXVI and CIII at the timing of termination is expanded and plotted in Fig. 3 (g). Prior to the CIII signal, the FeXVI signal started to increase from $t \sim 329.0$ s, and the discharge terminated at $t \sim 329.4$ s. Thus, the cause of the termination is the influx of iron. This impurity measurement coincides with an observation of sparks. Long pulse power injection from the 5.5-U port tends to cause sparks in the vicinity of the ECH antenna. The precise position and the source of the sparks are not clear yet.

As a reference, T_e and n_e profiles without e-ITB (black) of another long pulse (~41 min) ECH discharge #131054 ($R_{ax} = 3.6$ m, $B_t = 2.75$ T) [15] are plotted in Fig. 3 (c). The discharge #131054 was performed with nearly the same n_{e_ave} and P_{ECH} of ~350 kW (average of 321 kW and 374 kW timings due to the two-minute alternating operation of two of the four gyrotrons), while T_{e0} was ~2.7 keV. The 41 min discharge #131054 was sustained only with the EC-waves injected from the 2-O port. At the 321 kW timings, 154GHz#1 (2-OLL), 154GHz#2 (2-OUL), and 77GHz#1 (2-OLR) gyrotrons were operated. At the 374 kW timings, 154GHz#1, 154GHz#2, and 77GHz#2 (2-OUR) gyrotrons were operated.

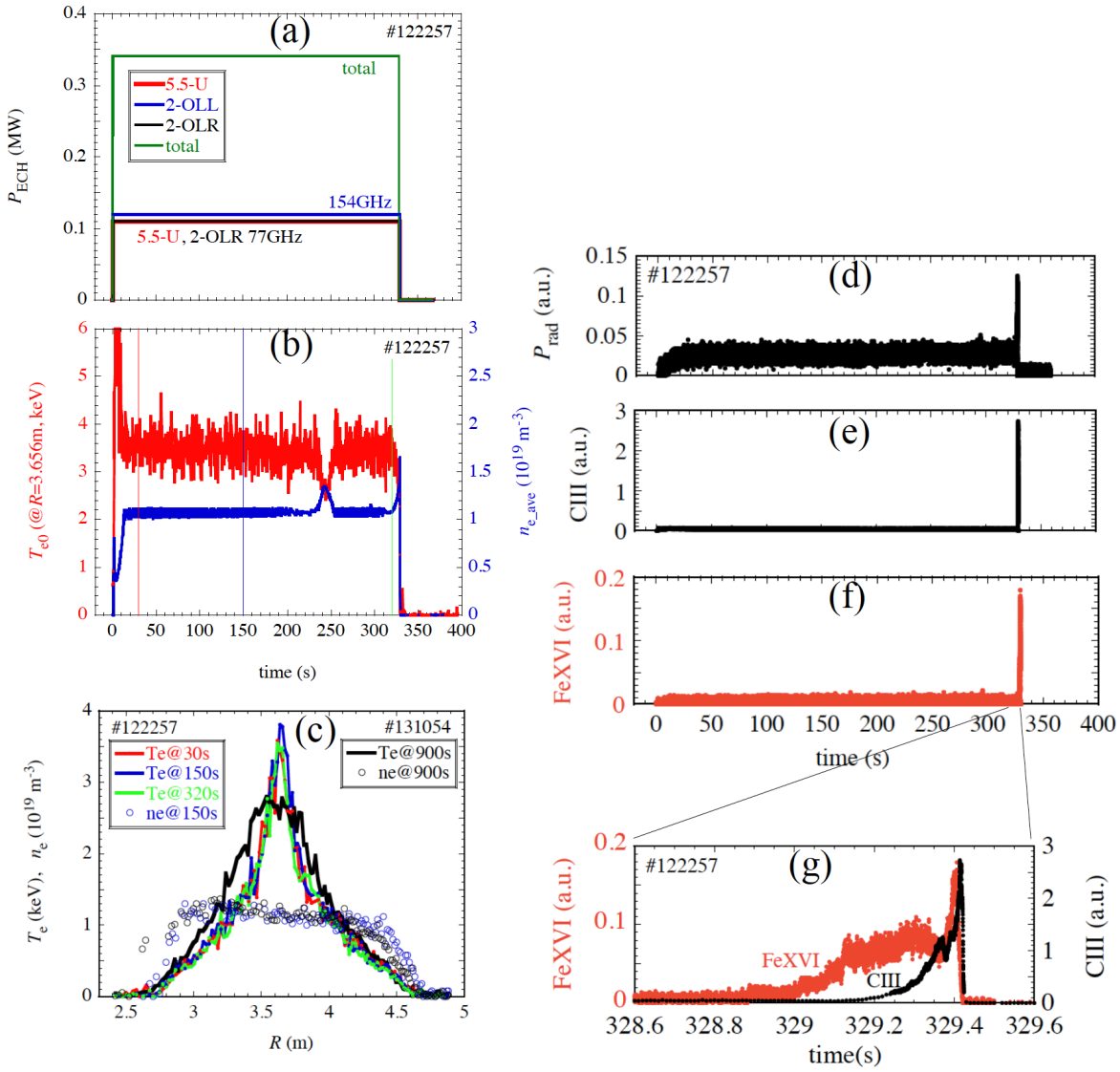

Figure 3. Waveforms in the ECH 330 s discharge with e-ITB, #122257: ECH power (a), central electron temperature (@R=3.656 m) and line average electron density (b), electron temperature profiles at 30 s, 150 s, and 320 s (c), radiation power (d), spectroscopy signals from carbon (e) and iron (f), and expansion of the carbon and the iron signals at the timing of plasma termination (g). An electron temperature profile in a discharge without e-ITB (#131054, at 900 s) is also plotted in (c).

Calculation of ECH power deposition using TRAVIS code indicates that the power deposition region (Fig. 2, colored in red) is at around the plasma center, and the deposition power density at the plasma center Q_{dep0} in #122257, ~2 MWm^{-3} as seen in Fig. 4, is 4 times higher than Q_{dep0} in #131054, ~0.5 MWm^{-3}. The power deposition profile in #131054 is nearly flat extending up to $\rho \sim 0.3$, differing from the highly peaked profile in #122257. Here, the magnetic configuration of #131054 and the resultant broader temperature profile were adopted expecting robust plasma against impurity influxes. The TRAVIS calculation indicates that the total absorbed power in #122257 is 322 kW so that the heating efficiency η is 95 %, and the total absorbed power in #131054 at 900 s is 371 kW, thus η is 99 %.

Radial distributions of electron thermal diffusivity coefficients in the discharges with and without e-ITB are evaluated using a transport coefficient evaluation tool based on the power balance, TR-snap [21], built in the integrated modelling code for three-dimensional configuration (TASK3D) [22], and are plotted in Fig. 5. Significant decrease in the thermal diffusivity coefficient at the plasma core

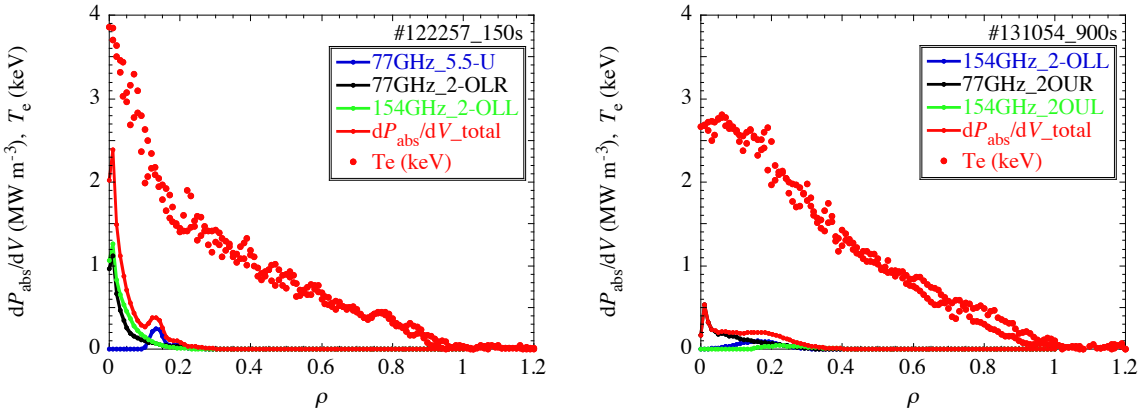

Figure 4. Distributions of absorbed ECH power per volume dP_{abs}/dV calculated with TRAVIS code and measured electron temperature profiles are plotted as functions of normalized minor radius for the with e-ITB discharge #122257 at 150 s and for the without e-ITB discharge #131054 at 900 s.

region inside $\rho \sim 0.2$ can be recognized, though fluctuations of the coefficients are large. The error bars of the electron thermal diffusivity coefficients are evaluated from the error bars of n_e and T_e measurements by Thomson scattering diagnostics. Because there is no T_i profile data in the discharges, the analysis was performed with an assumption of $T_i = T_e$. However, even if other T_i profiles, such as a parabolic profile with $T_{i0} = 1$ keV, are assumed, the profiles of thermal diffusivity in the core region are not significantly affected, because the absorbed ECH power at the core is much higher than the power flow from electrons to ions.

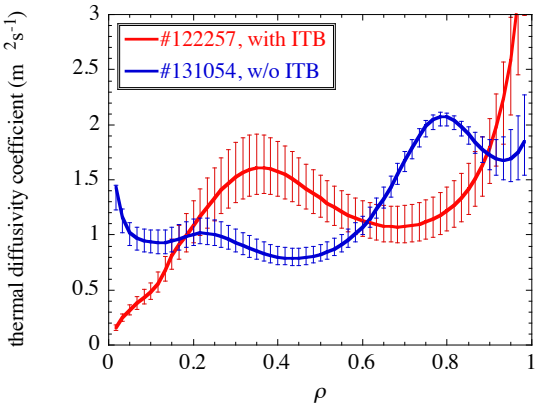

Figure 5. Radial distributions of electron thermal diffusivity coefficients in the discharges with and without e-ITB calculated with TR-snap code.

Comparison of the electron kinetic energies of the plasmas in the discharges with (#122257, R_{ax} = 3.65 m) and without (#131054, R_{ax} = 3.6 m) e-ITB shows that the kinetic energy in the case of without e-ITB is 1.24 times higher than that in the case of with e-ITB, mainly due to the difference in T_e profiles. The kinetic energies are evaluated using the T_e and n_e profile data. Though the electron temperature at the central region increases by the formation of e-ITB, the temperature decreases at the middle region. This may be explained mainly by the higher total absorbed power (371 kW compared with 322 kW as described above), the broader power deposition profile as seen in Fig. 4, and the lower thermal diffusivity coefficient at the middle region as seen in Fig. 5 in the discharge of without e-ITB. Also, the difference of R_{ax} in the discharges may have small contribution because the confinement property with R_{ax} = 3.6 m is slightly better than that with R_{ax} = 3.65 m in the LHD [23].

A temporal increase/decrease in the n_{e_ave}/T_{e0} at about t = 240 s was caused by a decrease in wall-pumping rate and a change of gas fuelling operations. For gas fuelling in the discharge, two helium mass flow controllers with large flow rate of up to 3,000 sccm (mass flow controller-L) and with small flow rate of up to 100 sccm (mass flow controller-S) were used. Each of the mass flow controllers furnishes mass flow meter-L and mass flow meter-S, respectively. The mass flow controller-L was mainly used at the plasma start-up timing for a pre-puffing. A control voltage of 1.5 V was applied to the mass flow controller-L for 440 ms from t = 0.87 s and the peak mass flow rate caused by the voltage application was 790 sccm. The mass flow controller-S was feedback controlled in order to maintain the plasma density at a set value of 1.1×10^{19} m^{-3} here. To apply basic gas fuelling, the mass flow controller-L was also used after the plasma startup by applying a control voltage of 2.4 V with 20

ms and 3.7 Hz pulses, although the mass flow meter-L did not respond to those short pulses. The n_{e_ave} and two signals of mass flow meters at the timing around t = 240 s are expanded and plotted in Fig. 6. As seen in the waveforms of n_{e_ave} and mass flow meter-S, the pace of feedback control became gradually slower and the flow rate became lower with time. This is evidence of a long timescale decrease in the wall-pumping rate. Then the 20 ms, 3.7 Hz pulse operation (gray area in Fig. 6) of the mass flow controller-L was stopped at t = 236.6 s. Though the flow rate signal of mass flow meter-L remained at the same noise level, practical gas fueling from the mass flow controller-L was stopped and the controllability of n_{e_ave} was recovered. This revealed that the wall-pumping was not saturated and continued to be active.

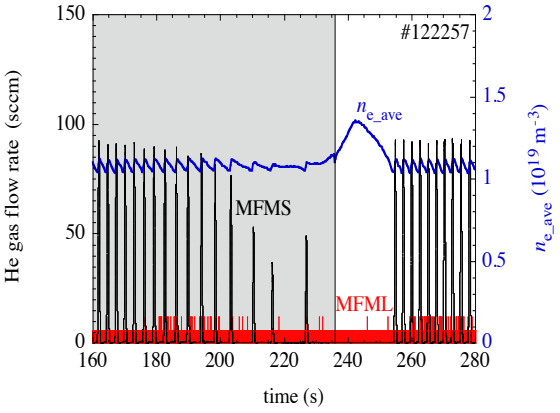

Figure 6. Waveforms of the line average electron density (blue) and signals of mass flow meter-L (red) and meter-S (black), at around the time when the temporal density increase occurred.

Even when n_{e_ave} reached its peak value of 1.35×10^{19} m^{-3} at t = 242 s, the e-ITB profile of the electron temperature was maintained, with decreased T_{e0} of ~2.5 keV.

Figure 7 shows the improvement in the plasma parameter region of the long pulse (> 5 min) ECH discharges (#56068, #117234, #122257, and #131054) owing to the increase in P_{ECH} and the formation of e-ITB. Formation of e-ITB and the increment in T_{e0} are dependent on Q_{dep0} and the electron density. In the discharge #56068, P_{ECH} was only 110 kW and the power of 84 GHz EC-wave was released from a waveguide opening installed at a bottom port (1.5-L) without using a focusing antenna system [12] in the on-axis second harmonic resonance condition for the 84 GHz waves. In the discharge #117234 with n_{e_ave} = ~0.7×10^{19} m^{-3} and the same magnetic configuration with that of #122257 (R_{ax} = 3.65 m, B_t = 2.712 T), three EC-wave powers (131 kW - 84 GHz from 1.5-L port, 155 kW - 77 GHz from a top port (9.5-U), and 110 kW - 77 GHz from the equatorial port 2-OLR) were applied, with the 84 GHz power continuously and the two 77 GHz powers alternately with 2 minute intervals. Q_{dep0} in the periods of the equatorial port injections is evaluated as 0.8 MWm^{-3}, while Q_{dep0} in the periods of the top port injections is 0 MWm^{-3} (off-axis heating at around ρ ~ 0.25). Only in the periods with Q_{dep0} = 0.8 MWm^{-3}, e-ITBs are formed and the increment of T_{e0} achieves ~1.1 keV, that is, an increment of ~65% from the T_{e0} of ~1.7 keV without e-ITB. In the case of n_{e_ave} = 1.1×10^{19} m^{-3} (#122257 and #131054), the increment of T_{e0} is ~30 %.

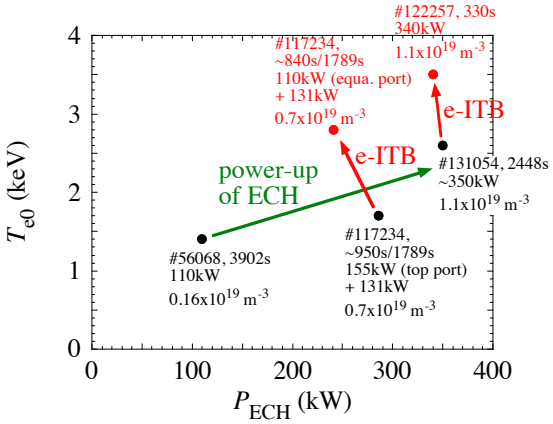

Figure 7. Improvements in line average electron density and central electron temperature of long pulse discharges over 5 min sustained with ECH, due to an increase in ECH power and/or formation of electron internal transport barrier. Shot number, duration time, and line average electron density are noted near the data points.

The T_e profiles at a timing of on-axis heating (red) and at a timing of off-axis heating (black) in the discharge #117234 are plotted in Fig. 8. The T_e profile in the discharge #122257 is also plotted for comparison. Under the same magnetic field configuration of the two discharges, a change of ECH power deposition from off-axis to on-axis results in a generation of e-ITB. Under the same on-axis

ECH condition, an increase of the deposition power density results in higher temperature not only at the peaked core region inside the transport barrier, but also at the entire region of the plasma. Thus, it is worth emphasizing that, in the LHD and other stellarators, the generation of e-ITB is caused by concentrated on-axis ECH achieved by an appropriate combination of R_{ax}, B_t, and EC-wave beam direction settings. The e-ITB is generated when the collisionality at the plasma core region is reduced enough for a transition from ion root, characterized by small radial electric field, to electron root characterized by large positive radial electric field [16, 17].

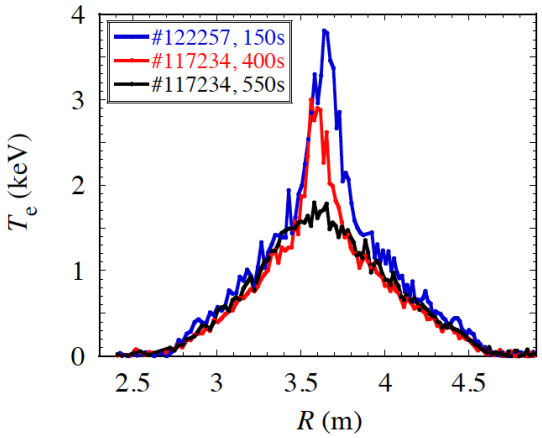

Figure 8. Electron temperature profiles in the discharges #117234 (red: at a period with on-axis ECH, black: at a period with off-axis ECH) and #122257 (blue: at t = 150s, the same data with that in Fig. 3 (c)).

4. Conclusions and future prospects

In recent years, long pulse discharges in the LHD have shown significant progress in sustaining plasmas with higher temperatures and densities, especially with improved confinement state (e-ITB). Plasmas having e-ITB with n_{e_ave} of 1.1×10^{19} m^{-3} are stably sustained for more than 5 min by 340 kW ECH power without any serious problem. Similar to the short pulse discharges, center-focused ECH power deposition generates and sustains the e-ITBs without degradation during the long pulse discharges. Due to the formation of e-ITBs, T_{e0} increased by 30 % or by 65 %. In the former case with $n_{e\_ave} = 1.1\times10^{19}$ m^{-3}, T_{e0} was improved to ~3.5 keV while T_{e0} of another discharge with the same n_{e_ave} but without e-ITB was ~2.7 keV. In the latter case with lower n_{e_ave} of $\sim0.7\times10^{19}$ m^{-3}, T_{e0} was improved to ~2.8 keV from ~1.7 keV. Further improved plasma parameters will be achieved by improvement in long pulse gyrotron operation and the resultant increase in heating power.

Performing longer discharges having e-ITB up to a few tens of minutes in the LHD will be possible by changing the method of power injections. The 5 min e-ITB discharge was terminated due to sparks which occurred near the ECH power injection antenna at 5.5-U port. However, this is not an essential problem, but is a problem specific to the LHD. Though the precise position and cause of the sparks are not clear yet, usage of power injection systems connected to the antennas installed in the equatorial port, instead of the power injection system connected to the 5.5-U antenna, would be able to extend the duration time of e-ITB discharges.

Acknowledgments

The authors would like to express their gratitude to the NIFS staff for performing the LHD experiments. This work was supported by the collaboration research programs of NIFS (NIFS13KLPR016) and the NIFS grants ULRR701 and 804.

References

[1] Yamada H *et al* 2011 *Nucl. Fusion* **51** 094021

[2] Kaneko O *et al* 2013 *Nucl. Fusion* **53** 104015

[3] Ida K *et al* 2015 *Nucl. Fusion* **55** 104018

[4] Bigot B *et al* 2016 *Proc. 26th Int. Conf. on Fusion Energy (Kyoto)* OV/1-2

[5] Kumazawa R *et al* 2010 *Fusion Sci. Technol*. **58** 524

[6] Mutoh T *et al* 2013 *Nucl. Fusion* **53** 063017

[7] Kasahara H *et al* 2014 *Phys. Plasmas* **21** 061505
[8] Kasahara H *et al* 2014 *Proc. 25th Int. Conf. on Fusion Energy (St. Petersburg)* EX/7-3
[9] Houtte D *et al* 2004 *Nucl. Fusion* **44** L11
[10] Wan B N *et al* 2016 *Proc. 26th Int. Conf. on Fusion Energy (Kyoto)* OV/2-2
[11] Gong X *et al* 2017 *Plasma Sci. Technol*. **19** 032001
[12] Yoshimura Y *et al* 2005 *J. Phys. Conf. Ser*. **25** 189
[13] Yoshimura Y *et al* 2010 *Fusion Sci. Technol*. **58** 551
[14] Yoshimura Y *et al* 2015 *EPJ Web Conf*. **87** 02020
[15] Yoshimura Y *et al* 2016 *Nucl. Fusion* **56** 046005
[16] Yokoyama M *et al* 2007 *Nucl. Fusion* **47** 1213
[17] Shimozuma T *et al* 2010 *Fusion Sci. Technol*. **58** 38
[18] Motojima G *et al* 2015 *J. Nucl. Mat.* **463** 1080
[19] Marushchenko N B *et al* 2011 *Phys. Plasmas* **18** 032501
[20] Suzuki C *et al* 2013 *Plasma Phys. Control. Fusion* **55** 014016
[21] Seki R *et al* 2011 *Plasma Fusion Res.* **6** 2402081
[22] Yokoyama M *et al* 2014 *Plasma Fusion Res*. **9** 3402017
[23] Yamada H *et al* 2001 *Plasma Phys. Control. Fusion* **43** A55